Supplement of Atmos. Chem. Phys. Discuss., 15, 30409–30471, 2015
http://www.atmos-chem-phys-discuss.net/15/30409/2015/
doi:10.5194/acpd-15-30409-2015-supplement

Atmospheric Chemistry and Physics Discussions

Supplement of

In situ secondary organic aerosol formation from ambient pine forest air using an oxidation flow reactor

B. B. Palm et al.

Correspondence to: J. L. Jimenez (jose.jimenez@colorado.edu)

S1 Correction for particle diffusion to sampling line walls

AMS and SMPS particle concentrations were corrected for diffusion losses to the walls of the inlet sampling lines, estimated using the Max Planck Institute for Chemistry's Particle Loss Calculator (von der Weiden et al., 2009). The sampling lines were constructed from a mixture of 3/8" and 1/4" OD copper tubing. The ambient air sampling line contained a $PM_{2.5}$ cyclone impactor at the inlet. The total length of tubing between the cyclone/OFR and AMS/SMPS was approximately 8 m, with a total residence time of about 9 s. The transmission curve used to correct for line losses is shown in Fig. S1. Estimates for particle losses in the ambient sampling line and in the OFR sampling line were similar, so a single transmission curve is applied to all data. The transmission curve was applied to SMPS size distributions to determine particle volume lost to the inlet walls. This volume was added to the AMS species in the same ratio that the species volumes were measured by the AMS. Mass was estimated from volume using densities of 1.52 g cm^{-3} for chloride and 1.75 g cm^{-3} for sulfate, ammonium, and nitrate AMS aerosol species (DeCarlo et al., 2004; Salcedo et al., 2006; Lide, 2013), and a parameterization using elemental composition to estimate the density of OA (Kuwata et al., 2012). The combination of the sampling line particle loss correction and the AMS lens transmission correction (discussed in Sect. S3) added an average of 4% to the ambient OA, and an average of 12% to the OA measured after 0.4–1.5 days of aging (when the corrections were largest).

S2 Determination of AMS collection efficiency (CE)

CE is typically variable between 0.5 and 1, depending on composition, as detailed in Middlebrook et al. (2012). To our knowledge, ambient AMS measurements with a constant CE of ~1 have been reported in two prior studies in forested environments: during the wet season in the remote Amazon forest at the Amazonian Aerosol Characterization Experiment 2008 (Chen et al., 2015), and South American Biomass Burning Analysis (SAMBBA) experiment during the dry season and dry-to-wet transition period in the southwestern Amazon rainforest in 2012 (Brito et al., 2014). Here, we assessed CE by comparing AMS measurements with an SMPS that sampled from the same inlet. This SMPS measurement was validated by an intercomparison with four other calibrated and independently-operated SMPS instruments, as well as three CPC total particle number measurements, that sampled concurrently at the same research site. Fig. S2 shows that CE = 1 was required to match the AMS and SMPS measurements.

One concern was that the CE would change after oxidation in the OFR, due to changes in the aerosol composition and properties. A change in CE would result in a change in the slope of AMS vs. SMPS

volume. However, we did not observe such a change, as seen in the comparison of total aerosol volume measured after the OFR in the left panel of Fig. S3. Occasionally, high concentrations of NH_4NO_3 were produced in the OFR from OH oxidation. During those times, the AMS measured up to several times more volume than the SMPS (implying a CE>>1). This is likely due to evaporation of the NH_4NO_3 in the SMPS, as the SMPS sample flow was diluted inside the DMA column, as well as between the DMA and the CPC. For this reason, these data are not included in the analysis of CE.

Fig. S4 shows total particle volume enhancements as quantified by both the AMS and the SMPS for the OFR185 method vs. photochemical age, split into daytime and nighttime, showing that the two instruments measured similar enhancements within the errors at all ages. Data in Figs. S2, S3, and S4 were corrected using the sampling inlet line particle transmission efficiency curve in Fig. S1 as well as a correction for the transmission of the AMS aerodynamic lens, discussed in Sect. S3.

S3 Determination of AMS aerodynamic lens transmission efficiency

As discussed in Sect. 3.5 and Fig. 9, OH oxidation of ambient air in the OFR often led to substantial new particle formation. The AMS aerodynamic lens is known to have less than 100% transmission at small sizes (Liu et al., 2007). A standard transmission curve has been suggested for correcting AMS data when lacking a determination of the transmission for the particular operating conditions of the AMS, referred to as case 0 here (Knote et al., 2011). However, it is preferable to use data from a specific experiment when available to make such a determination for specific operating condtitions. The lens transmission curve was estimated for the conditions in which the AMS was operated at the BEACHON-RoMBAS campaign by empirically finding the low particle size cutoff that resulted in the highest R^2 correlation of the AMS and SMPS total volume sampled through an OFR (including all data from unperturbed to the highest OH_{exp}). We tested a range of corrections, shown in Fig. S5. The results are shown in Table S1. Scatterplots of total volume and volume added for the base case (no correction) and the chosen case 2 correction are shown in Figs. S6 and S3, respectively. The combination of the sampling line particle loss correction and the AMS lens transmission correction added an average of 4% to the ambient OA, and an average of 12% to the total OA measured after 0.4–1.5 days of aging in the reactor (when the corrections were largest).

Finally, to account for any particle losses on the surfaces inside the OFR, the aerosol mass measured in the OFR when no oxidant was added was adjusted to be equal to the concurrent ambient aerosol data, which was interpolated from the measurements immediately before and after the OFR data. Aerosol

was sampled through the OFR with no added oxidant approximately every 2 hours. The OFR data for which oxidant concentrations were increased were corrected by multiplying by the average ratio of ambient aerosol mass to aerosol mass measured through the OFR without added oxidant. This correction was small, increasing the mass of OFR data by 4%, similar in magnitude to the loss of particles in the sampling lines and aerodynamic lens.

S4 In-canopy vs. 25 m height PTR-TOF-MS measurements

The primary PTR-TOF-MS dataset from BEACHON-RoMBAS was measured from an inlet located on a tower at 25 m, above the average canopy height of 16 m (Ortega et al., 2014). The OFR was located within the canopy at approximately 4 m height. Occasionally, concurrent PTR-TOF-MS measurements were available from the 25 m height and either through the OFR (1–6 and 8–10 August) or from a 1 m high inlet (19–21 August). Scatterplots of in-canopy (OFR or 1 m) vs. 25 m inlet MT, SQT, MBO+isoprene, and toluene+*p*-cymene concentrations are shown in Fig. S8. In-canopy concentrations were observed to be 1.9, 5.9, 1.4, and 1.2 times higher than at 25 m for those four compounds, respectively, and these ratios were used to estimate a campaign-long time series of in-canopy concentrations using the 25 m measurements. The correlations are high for MT, toluene, and MBO+isoprene (R^2=0.80-0.82), but the correlation for SQT is R^2=0.12. This low correlation adds uncertainty to the estimation of in-canopy SQT concentrations. However, this will have only a minor effect on the predicted SOA formation from VOCs (Sect. 3.6.1) since on average only 5% of the predicted SOA formation came from SQT.

References

Brito, J., Rizzo, L. V., Morgan, W. T., Coe, H., Johnson, B., Haywood, J., Longo, K., Freitas, S., Andreae, M. O. and Artaxo, P.: Ground-based aerosol characterization during the South American Biomass Burning Analysis (SAMBBA) field experiment, Atmos. Chem. Phys., 14, 12069–12083, 2014.

Chen, Q., Farmer, D. K., Rizzo, L. V., Pauliquevis, T., Kuwata, M., Karl, T. G., Guenther, A., Allan, J. D., Coe, H., Andreae, M. O., Pöschl, U., Jimenez, J. L., Artaxo, P. and Martin, S. T.: Fine-mode organic mass concentrations and sources in the Amazonian wet season (AMAZE-08), Atmos. Chem. Phys., 15, 3687–3701, doi:10.5194/acp-15-3687-2015, 2015.

DeCarlo, P. F., Slowik, J. G., Worsnop, D. R., Davidovits, P. and Jimenez, J. L.: Particle Morphology and Density Characterization by Combined Mobility and Aerodynamic Diameter Measurements. Part 1: Theory, Aerosol Sci. Technol., 38, 1185–1205, doi:10.1080/027868290903907, 2004.

Knote, C., Brunner, D., Vogel, H., Allan, J., Asmi, A., Äijälä, M., Carbone, S., van der Gon, H. D., Jimenez, J. L., Kiendler-Scharr, A., Mohr, C., Poulain, L., Prévôt, A. S. H., Swietlicki, E. and Vogel, B.: Towards an

online-coupled chemistry-climate model: evaluation of trace gases and aerosols in COSMO-ART, Geosci. Model Dev., 4, 1077–1102, 2011.

Kuwata, M., Zorn, S. R. and Martin, S. T.: Using elemental ratios to predict the density of organic material composed of carbon, hydrogen, and oxygen., Environ. Sci. Technol., 46, 787–94, doi:10.1021/es202525q, 2012.

Lide, D. R.: CRC Handbook of Chemistry and Physics, 94th Edition, 2013-2014., 2013.

Liu, P. S. K., Deng, R., Smith, K. a., Williams, L. R., Jayne, J. T., Canagaratna, M. R., Moore, K., Onasch, T. B., Worsnop, D. R. and Deshler, T.: Transmission efficiency of an aerodynamic focusing lens system: Comparison of model calculations and laboratory measurements for the Aerodyne Aerosol Mass Spectrometer, Aerosol Sci. Technol., 41, 721–733, doi:10.1080/02786820701422278, 2007.

Middlebrook, A. M., Bahreini, R., Jimenez, J. L. and Canagaratna, M. R.: Evaluation of Composition-Dependent Collection Efficiencies for the Aerodyne Aerosol Mass Spectrometer using Field Data, Aerosol Sci. Technol., 46, 258–271, doi:10.1080/02786826.2011.620041, 2012.

Ortega, J., Turnipseed, A., Guenther, A. B., Karl, T. G., Day, D. A., Gochis, D., Huffman, J. A., Prenni, a. J., Levin, E. J. T., Kreidenweis, S. M., DeMott, P. J., Tobo, Y., Patton, E. G., Hodzic, a., Cui, Y. Y., Harley, P. C., Hornbrook, R. S., Apel, E. C., Monson, R. K., Eller, A. S. D., Greenberg, J. P., Barth, M. C., Campuzano-Jost, P., Palm, B. B., Jimenez, J. L., Aiken, a. C., Dubey, M. K., Geron, C., Offenberg, J., Ryan, M. G., Fornwalt, P. J., Pryor, S. C., Keutsch, F. N., DiGangi, J. P., Chan, A. W. H., Goldstein, A. H., Wolfe, G. M., Kim, S., Kaser, L., Schnitzhofer, R., Hansel, a., Cantrell, C. a., Mauldin, R. L. and Smith, J. N.: Overview of the Manitou Experimental Forest Observatory: site description and selected science results from 2008 to 2013, Atmos. Chem. Phys., 14, 6345–6367, doi:10.5194/acp-14-6345-2014, 2014.

Salcedo, D., Onasch, T. B., Dzepina, K., Canagaratna, M. R., Zhang, Q., Huffman, J. A., DeCarlo, P. F., Jayne, J. T., Mortimer, P., Worsnop, D. R., Kolb, C. E., Johnson, K. S., Zuberi, B., Marr, L. C., Volkamer, R., Molina, L. T., Molina, M. J., Cardenas, B., Bernabe, R. M., Marquez, C., Gaffney, J. S., Marley, N. A., Laskin, A., Shutthanandan, V., Xie, Y., Brune, W., Lesher, R., Shirley, T., Jimenez, J. L., Salcedo, D., Onasch, T. B., Dzepina, K., Canagaratna, M. R., Zhang, Q., Huffman, J. A., DeCarlo, P. F., Jayne, J. T., Mortimer, P., Worsnop, D. R., Kolb, C. E., Johnson, K. S., Zuberi, B., Marr, L. C., Volkamer, R., Molina, L. T., Molina, M. J., Cardenas, B., Bernabe, R. M., Marquez, C., Gaffney, J. S., Marley, N. A., Laskin, A., Shutthanandan, V., Xie, Y., Brune, W., Lesher, R., Shirley, T., Jimenez, J. L., Salcedo, D., Onasch, T. B., Dzepina, K., Canagaratna, M. R., Zhang, Q., Huffman, J. A., DeCarlo, P. F., Jayne, J. T., Mortimer, P., Worsnop, D. R., Kolb, C. E., Johnson, K. S., Zuberi, B., Marr, L. C., Volkamer, R., Molina, L. T., Molina, M. J., Cardenas, B., Bernabe, R. M., Marquez, C., Gaffney, J. S., Marley, N. A., Laskin, A., Shutthanandan, V., Xie, Y., Brune, W., Lesher, R., Shirley, T., Bernabé, R. M., Márquez, C., Gaffney, J. S., Marley, N. A., Laskin, A., Shutthanandan, V., Xie, Y., Brune, W., Lesher, R., Shirley, T., Jimenez, J. L., Bernabe, R. M., Marquez, C., et al.: Characterization of ambient aerosols in Mexico City during the MCMA-2003 campaign with Aerosol Mass Spectrometry: results from the CENICA Supersite, Atmos. Chem. Phys., 6, 925–946, doi:10.5194/acp-6-925-2006, 2006.

Tsimpidi, A. P., Karydis, V. A., Zavala, M., Lei, W., Molina, L., Ulbrich, I. M., Jimenez, J. L. and Pandis, S. N.: Evaluation of the volatility basis-set approach for the simulation of organic aerosol formation in the Mexico City metropolitan area, Atmos. Chem. Phys., 10, 525–546, doi:10.5194/acp-10-525-2010, 2010.

Von der Weiden, S.-L., Drewnick, F. and Borrmann, S.: Particle Loss Calculator – a new software tool for the assessment of the performance of aerosol inlet systems, Atmos. Meas. Tech., 2, 479–494, doi:10.5194/amt-2-479-2009, 2009.

Table S1. Slope and correlation values for a comparison of AMS vs. SMPS volume, when applying aerodynamic lens transmission correction curves 0-5 (shown in Fig. S5) or no correction (base case).

Total Volume			**Added Volume**		
Case	Slope	R^2	Case	Slope	R^2
0	1.056	0.85	0	1.446	0.77
1	1.036	0.85	1	1.341	0.77
2	1.017	0.86	2	1.219	0.75
3	1.001	0.85	3	1.107	0.70
4	0.989	0.84	4	1.032	0.65
5	0.983	0.82	5	0.997	0.61
base	0.981	0.81	base	0.986	0.58

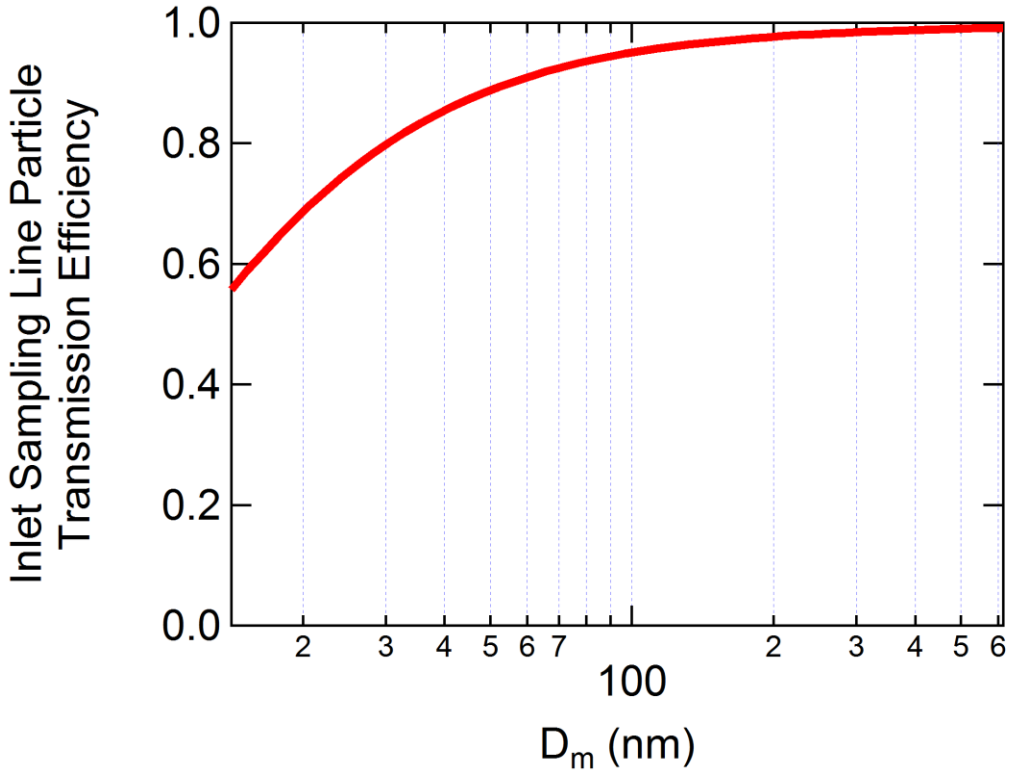

Fig. S1. OFR and ambient inlet sampling line particle transmission efficiency, estimated using the Max Planck Institute for Chemistry Particle Loss Calculator (von der Weiden et al., 2009). This transmission curve was used to correct SMPS size distributions for particle losses in the sampling lines. Particle losses to surfaces inside the OFR are discussed in Sect. S3.

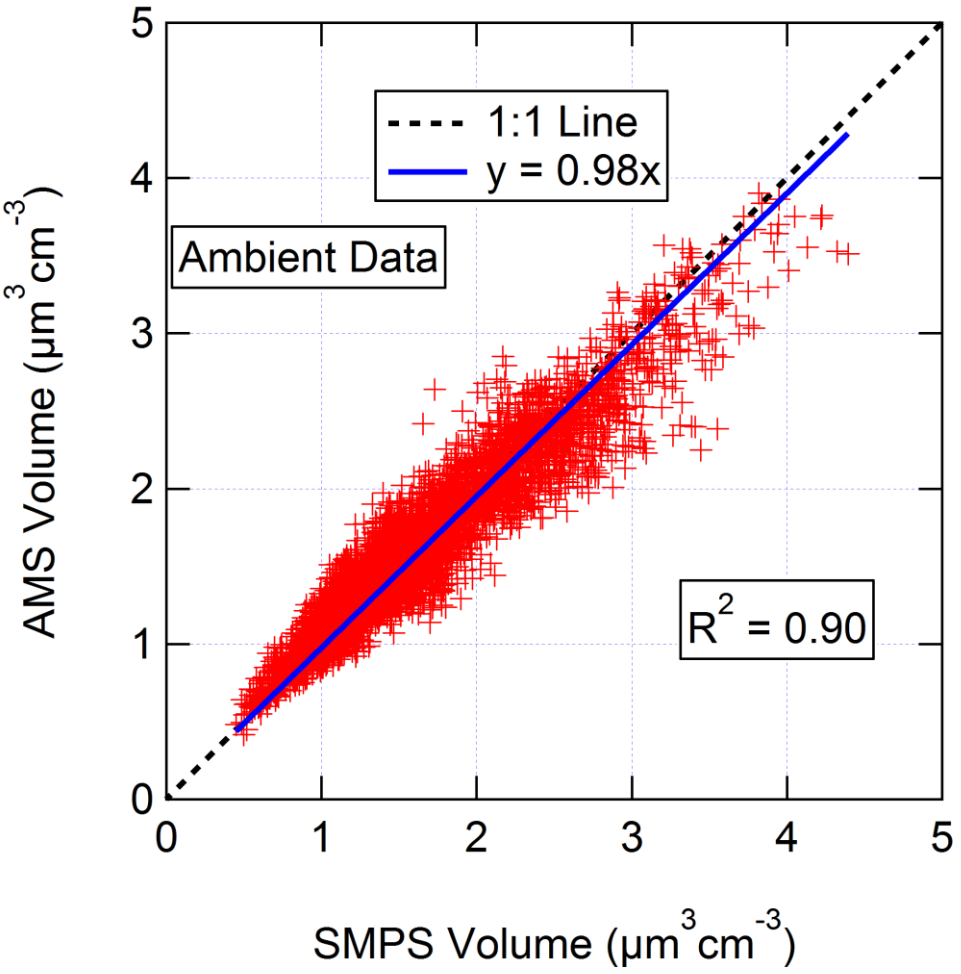

169

170 Fig. S2. Scatter plot of ambient aerosol volume measurements from AMS vs. SMPS with regression line.
171 AMS data was calculated using CE=1. AMS volume was estimated using densities of 1.52 g cm^{-3} for
172 chloride, 1.75 g cm^{-3} for sulfate, ammonium, and nitrate (DeCarlo et al., 2004; Salcedo et al., 2006; Lide,
173 2013), and a parameterization using elemental composition to estimate the density of OA (Kuwata et al.,
174 2012). All data is shown without the LVOC fate correction.

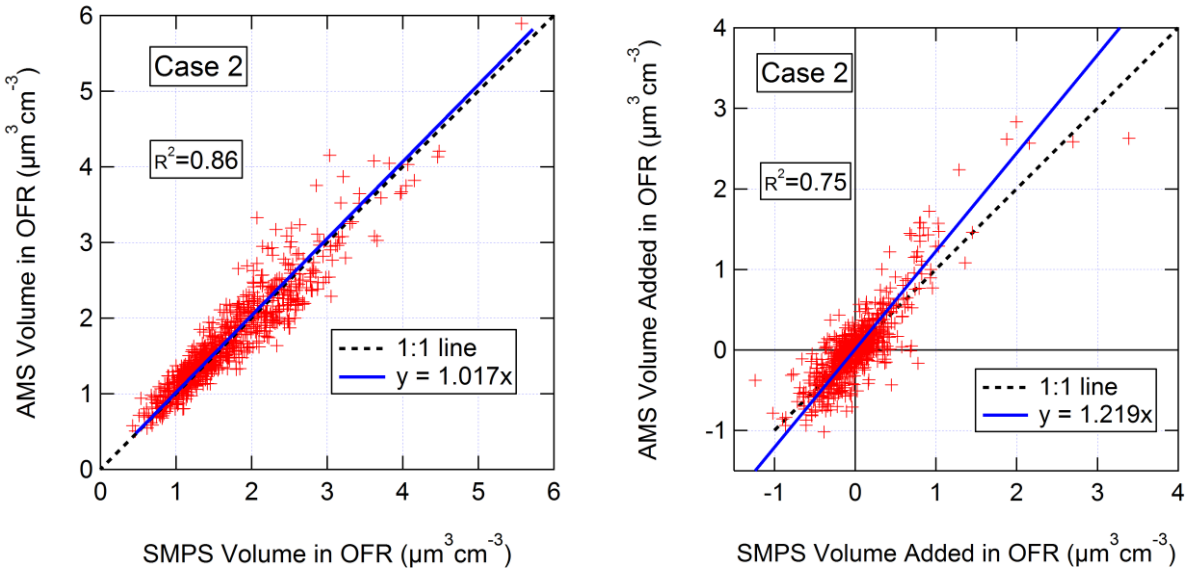

175

176 Fig. S3. Scatter plot of aerosol volume and volume added after OH aging from AMS vs. SMPS. AMS
177 volume was estimated using densities of 1.52 for chloride, 1.75 for sulfate, ammonium, and nitrate
178 (DeCarlo et al., 2004; Salcedo et al., 2006; Lide, 2013), and a parameterization using elemental
179 composition to estimate the density of OA (Kuwata et al., 2012). Data is shown after correction for
180 particle transmission losses in the AMS aerodynamic lens according to the case 2 correction in Fig. S5. All
181 data is shown without the LVOC fate correction.

182

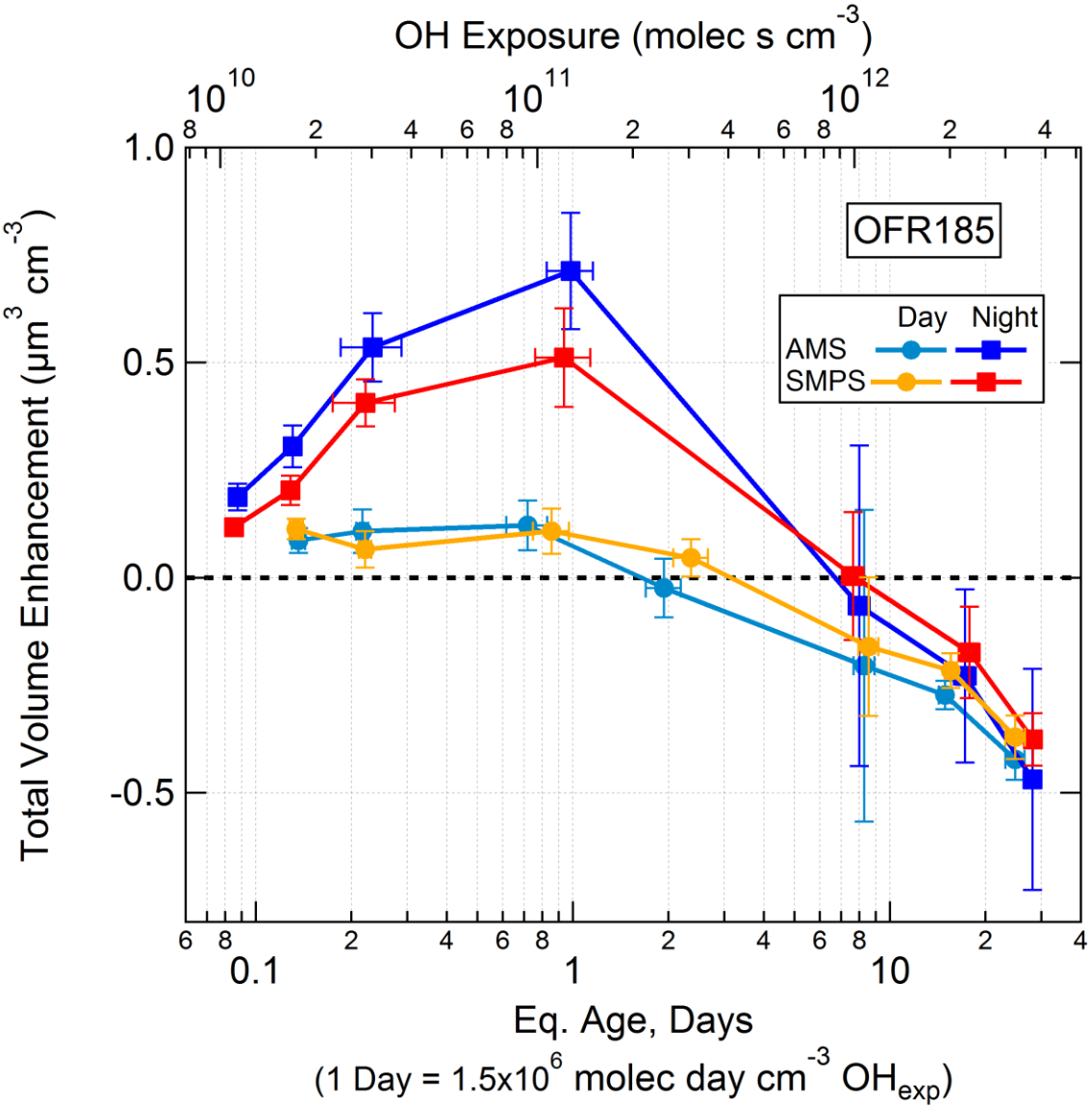

183

184 Fig. S4. Total particle volume enhancement as measured by the AMS and SMPS as a function of
185 photochemical age, split into daytime (08:00–20:00 local time) and nighttime (20:00–08:00 local time)
186 data. AMS volume was estimated using densities of 1.52 g cm^{-3} for chloride, 1.75 g cm^{-3} for sulfate,
187 ammonium, and nitrate (DeCarlo et al., 2004; Salcedo et al., 2006; Lide, 2013), and a parameterization
188 using elemental composition to estimate the density of OA (Kuwata et al., 2012). All data is shown
189 without the LVOC fate correction. Error bars represent the standard error of the mean of each quantile
190 of data.

191

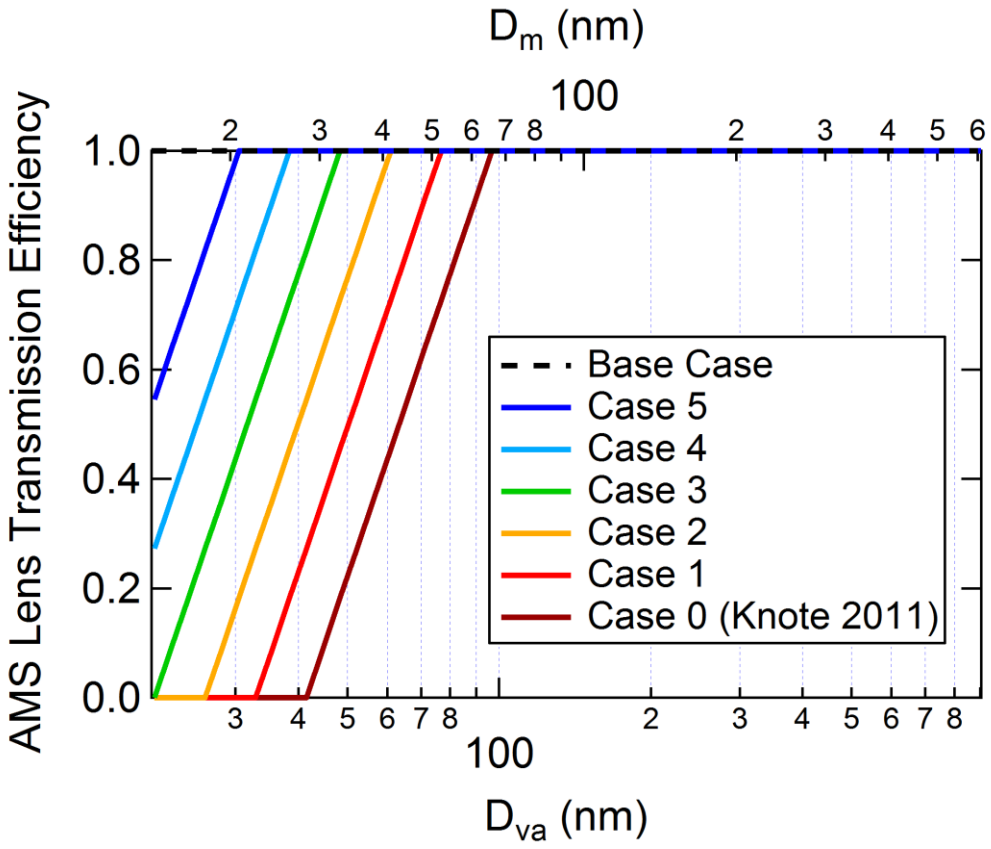

192

193 Fig. S5. Potential AMS aerodynamic lens transmission efficiency curves used to evaluate small particle
194 losses in the lens, as a function of vacuum aerodynamic diameter D_{va} and mobility diameter D_m. D_{va} was
195 converted to D_m assuming a density of 1.45 g cm^{-3} (the campaign average). Case 0 is the recommended
196 AMS lens transmission efficiency when no campaign-specific determination is possible (Knote et al.,
197 2011). Case 2 was chosen as the best fit for the data under the conditions during BEACHON-RoMBAS.

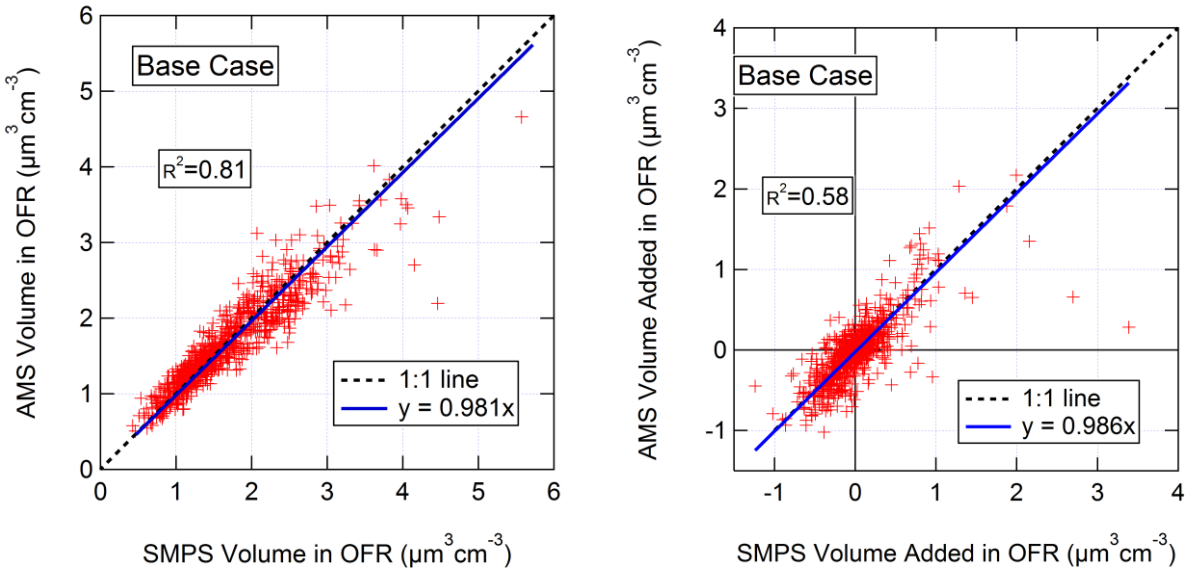

198
199

200 Fig. S6. Scatter plot of aerosol volume and volume added after OH aging from AMS vs. SMPS. AMS
201 volume was estimated using densities of 1.52 g cm^{-3} for chloride, 1.75 g cm^{-3} for sulfate, ammonium, and
202 nitrate (DeCarlo et al., 2004; Salcedo et al., 2006; Lide, 2013), and a parameterization using elemental
203 composition to estimate the density of OA (Kuwata et al., 2012). Data is shown for base case
204 (uncorrected) for particle transmission losses in the AMS aerodynamic lens according to Fig. S5. All data
205 is shown without the LVOC fate correction.

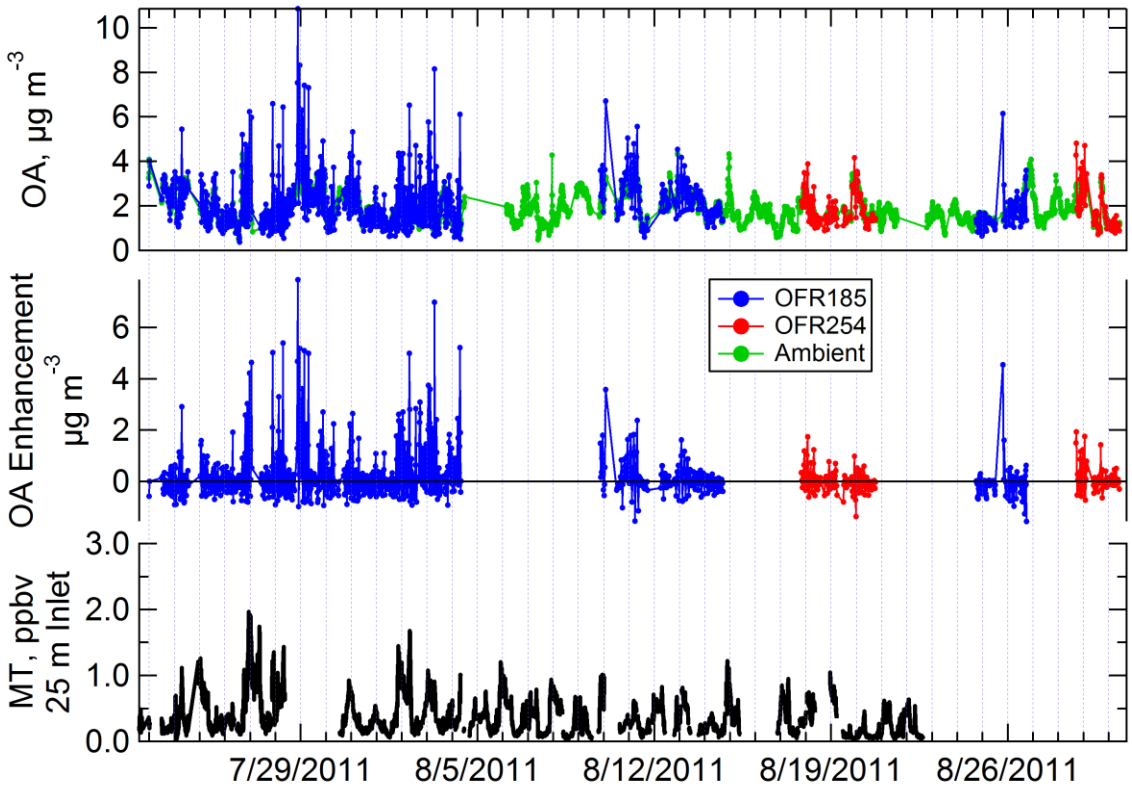

206

207 Fig. S7. Time series of ambient OA, total OA and OA enhancement for OFR185 and OFR254 methods,
208 and ambient MT (25 m inlet). The OA enhancements are not LVOC fate corrected here, and include all
209 ages.

210

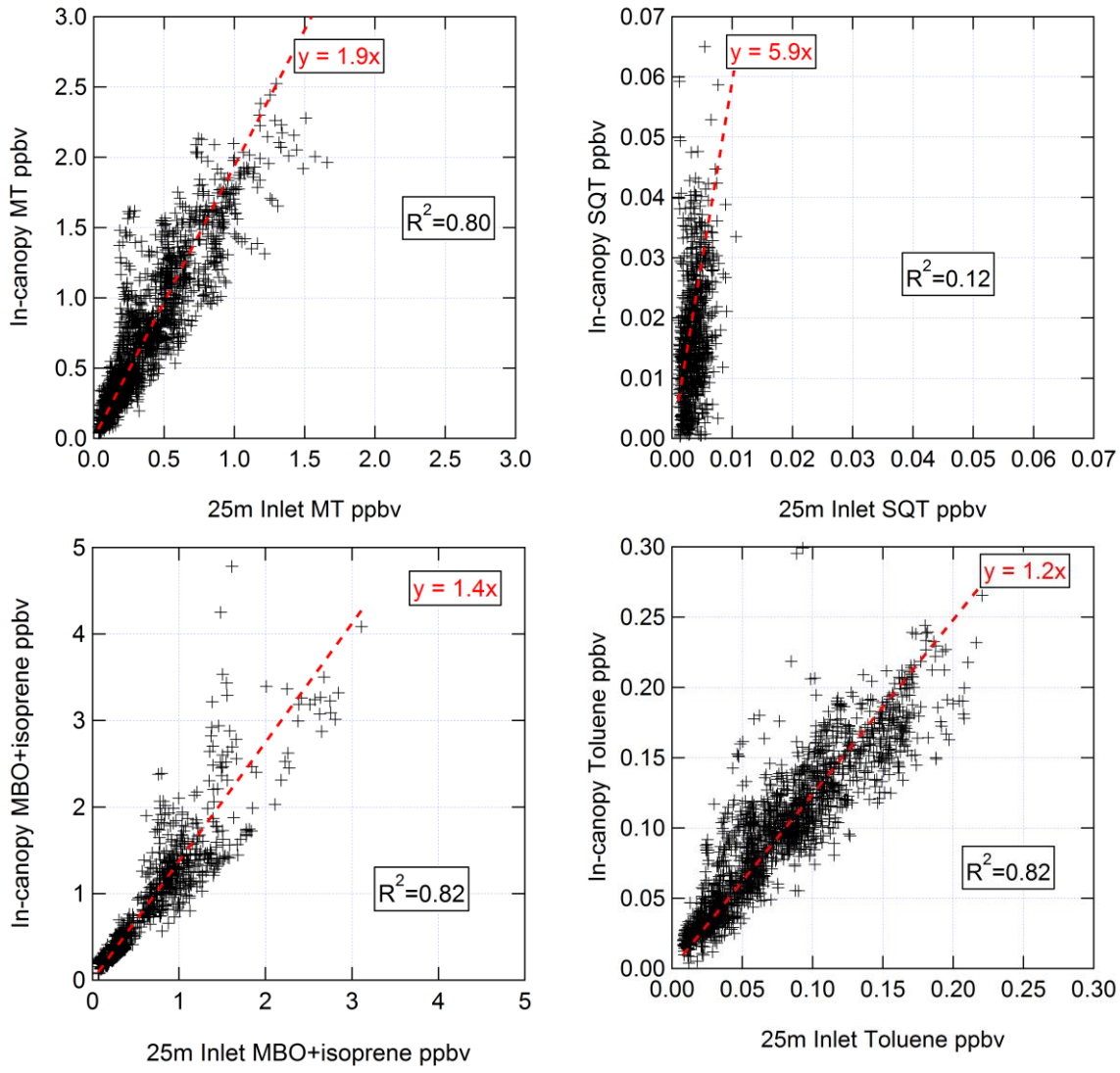

211

212 Fig. S8. Scatterplots of in-canopy (through OFR or 1 m inlet) vs. 25 m inlet for PTR-TOF-MS
213 measurements of MT, SQT, MBO+isoprene, and toluene. In-canopy concentrations were 1.9, 5.9, 1.4,
214 and 1.2 times higher than at 25 m, respectively.

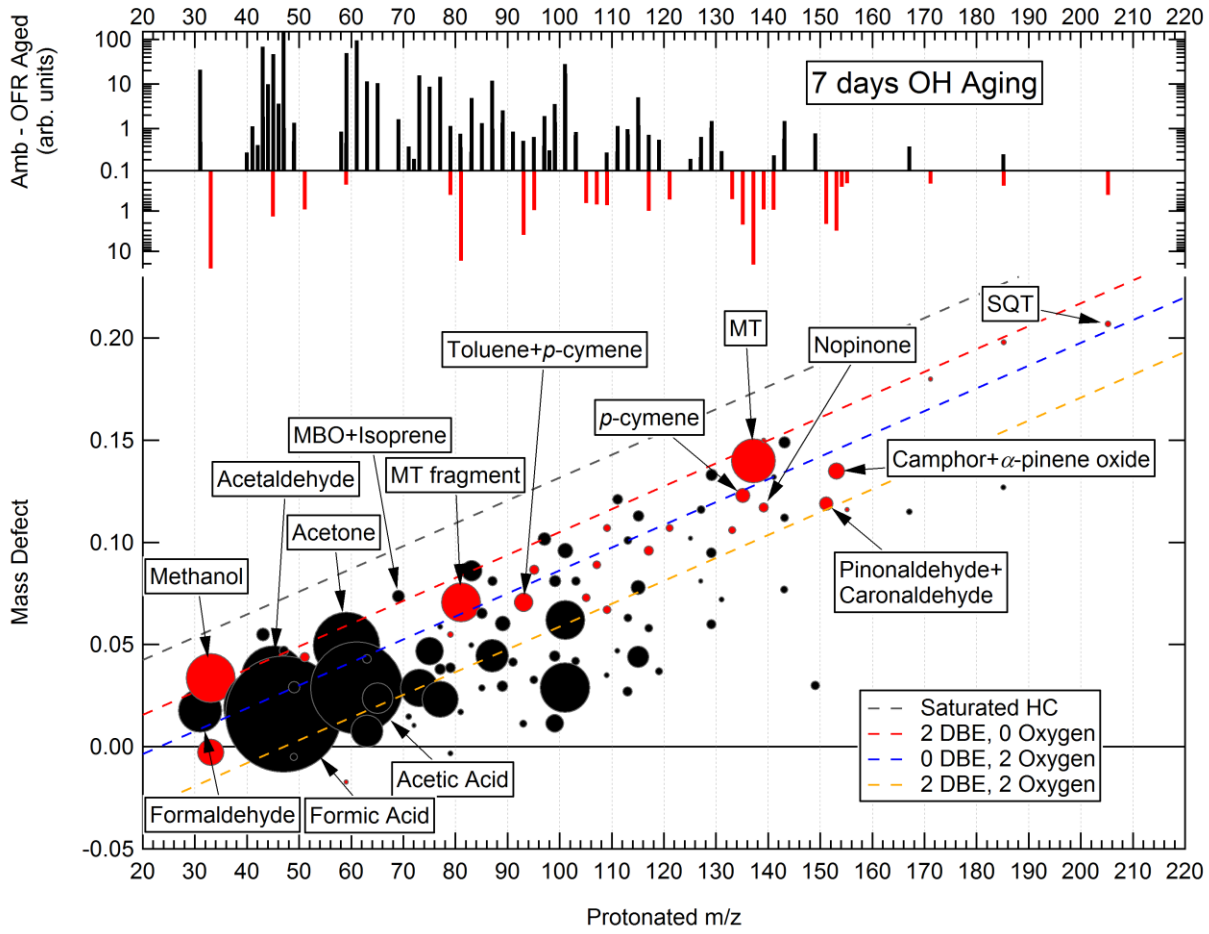

215

216 Fig. S9. The absolute changes of ions (signal after OH oxidation in the reactor minus ambient signal)
217 measured by the PTR-TOF-MS after 7 days of aging using the OFR185 method, shown as a difference
218 mass spectrum and in a mass defect diagram. The mass spectra are 10-min averages (5 min from each of
219 the two sample cycles used). The background-subtracted signals are shown in arbitrary units, not
220 corrected for differences in sensitivity of each compound due to the large number of compounds and
221 the inability to positively identify all of them. Prominent ions are labeled by name or elemental formula
222 assignments. Dashed lines representing molecules with varying double bond equivalents (DBE) or
223 number of oxygen atoms are shown for reference. A red marker signifies that the signal decreased due
224 to oxidation, while a black marker indicates where signal was greater after oxidation. The markers are
225 sized by the square root of the absolute change in signal at each peak after oxidation (i.e., marker area is
226 proportional to signal). Minor signals with absolute change of <0.2 arb. units or change of <20% of total
227 ambient signal are removed.

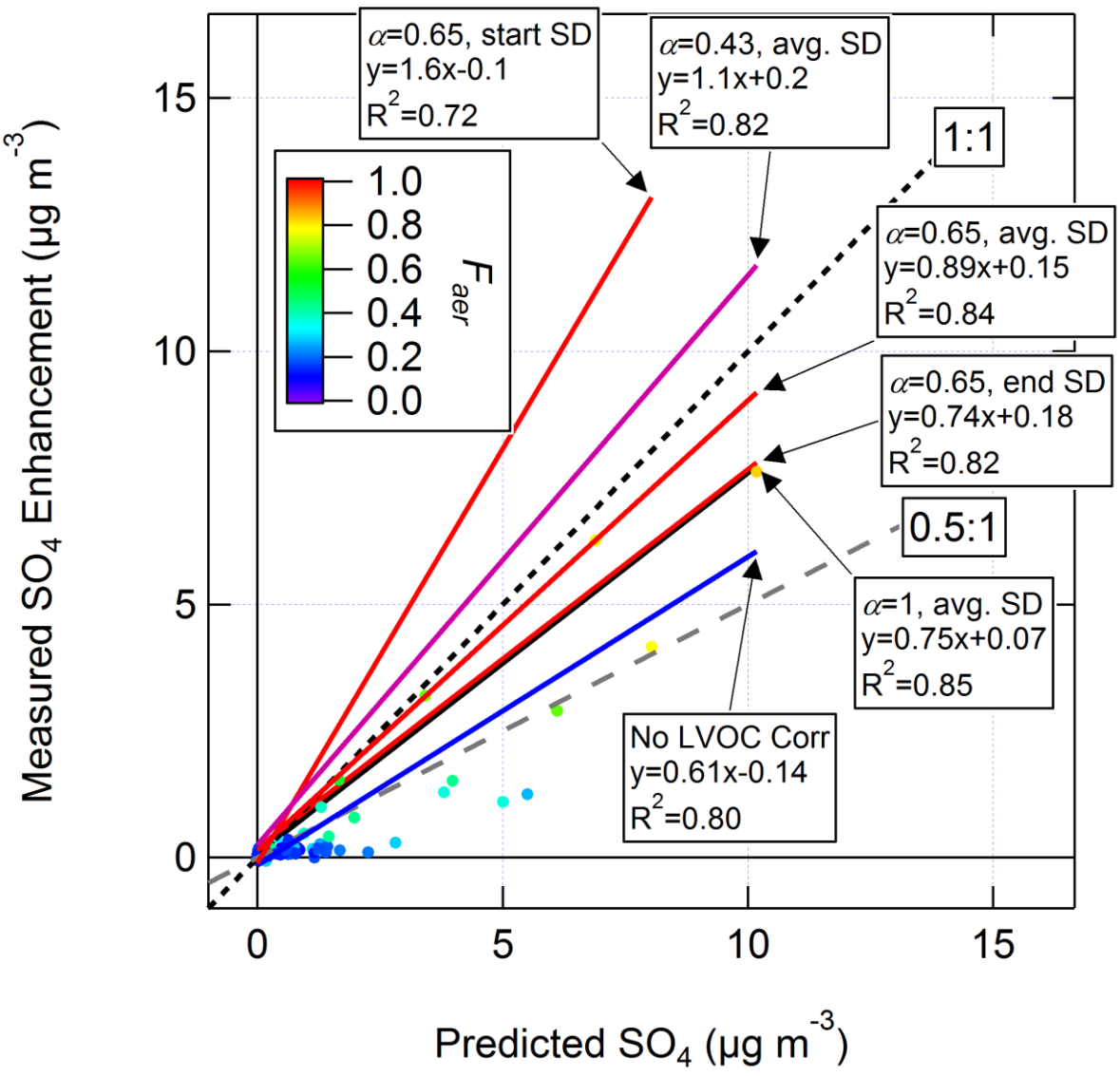

Fig. S10. Sensitivity study of the measured vs. predicted SO_4 formation after OH oxidation in the OFR vs. key uncertain parameters. The data points are colored by the fraction of H_2SO_4 predicted to condense on aerosols, calculated using α = 0.65 and the average of the SMPS size distributions (SD) measured before and after oxidation. Data are shown without applying the LVOC fate correction, along with linear fits that result from applying various sets of corrections including α = 0.43-1 and using the ambient (start), post-oxidation (end), or average SD to calculate the *CS*.

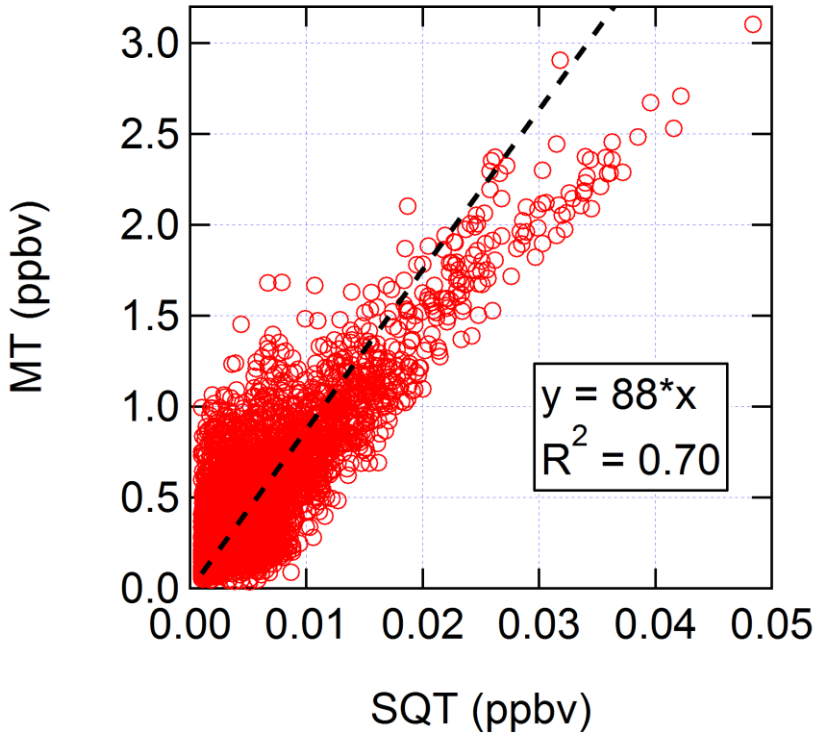

235

236 Fig. S11. Scatterplot of ambient MT vs. SQT concentrations measured by the PTR-TOF-MS at the 25 m

237 inlet above the canopy.

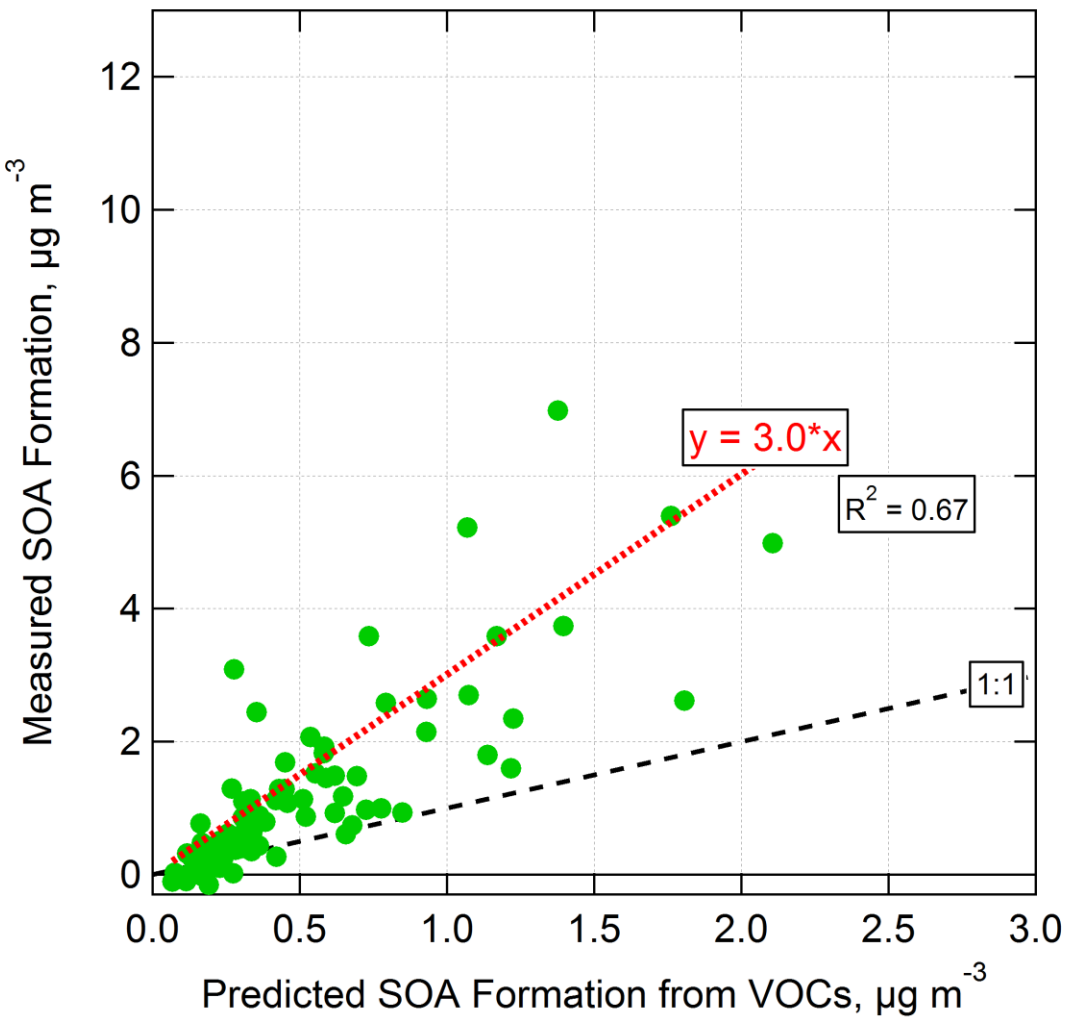

238

239 Fig. S12. Measured vs. predicted SOA formation from OH oxidation of ambient air in an OFR using the
240 OFR185 method. Only the range of photochemical ages with the highest SOA formation (0.4-1.5 eq.
241 days) was used. The LVOC fate correction was not applied. Predicted SOA formation was calculated by
242 applying OA concentration-dependent yields (average of 10.9%, 10.6%, 12.3%, and 1.4% for MT, SQT,
243 toluene, and isoprene, respectively, with average OA concentration of 2.9 µg m^{-3}) to VOCs reacted in the
244 OFR (Tsimpidi et al., 2010). The amount of reacted VOCs was estimated using OH_{exp} and ambient VOC
245 concentrations. If a non-zero y-intercept is allowed, the regression line becomes y = 3.9x – 0.7.